RSC Advances

PAPER

View Article Online
View Journal | View Issue

Cite this: *RSC Adv.*, 2020, **10**, 38663

Photocatalytic degradation of diphenhydramine in aqueous solution by natural dolomite†

Lihong Song,[a] Chunlin Yi,[a] Qingfeng Wu, *[a] Zhaohui Li, *[b] Weibin Zhang[a] and Hanlie Hong[c]

Natural dolomite, an inexpensive and vastly available natural material, was demonstrated as a potential heterogeneous photocatalyst for the efficient removal of diphenhydramine (DP) from aqueous solution under simulated solar light in this study. About 65% DP removal and 14% mineralization were achieved with dolomite as a catalyst after 75 min irradiation. The electron spin resonance analysis and scavenger experiments verified that $^1O_2$, $^{\bullet}OH$, and $O_2^{-\bullet}$ produced in the dolomite system were the main reactive species responsible for DP degradation. Furthermore, first-principle calculations combined with deoxygenation experiments were employed to elucidate the photocatalytic mechanism. The results revealed that the dolomite changed from an insulator to a semiconductor after partial substitution of Mg^{2+} by Fe^{2+}, suggesting that natural dolomite could act as a semiconductor photocatalyst in photoreactions. Under irradiation, photo-excited electrons and holes separate and migrate to the surface of dolomite, and subsequently react to form reactive species resulting in the DP degradation. Product studies demonstrated that the main degradation pathways of DP included hydroxylation of the aromatic ring as well as hydroxyl radical mediated oxidation of the alkylamine side chain. This work indicated that natural dolomite could be applied in water and wastewater treatment as a promising photocatalyst.

Received 2nd September 2020
Accepted 8th October 2020

DOI: 10.1039/d0ra07533g

rsc.li/rsc-advances

1. Introduction

Pharmaceutically active compounds (PhACs) are a class of compounds used to prevent, control, and treat diseases and to promote human and animal health. Due to widespread consumption and incomplete removal in conventional wastewater treatment plants, PhACs are constantly introduced into the environment *via* discharges of wastewater and direct runoff, resulting in their occurrence in environmental waters.[1–3] Prevalence and long-term persistence of trace PhACs in aquatic environments can cause potential risks to aquatic organisms and human health.[4–6]

Diphenhydramine (DP), an H1-histamine receptor antagonist, is commonly used to treat allergies, hives, itching and insomnia, and also used as an analgesic adjuvant in cancer pain.[7] Previous reports showed its presence in wastewater influent and effluent and surface water.[8,9] Therefore, to develop effective techniques for the removal of DP from aqueous solution is of great environmental interest.

In recent years, advanced oxidation processes (AOPs), as an environmental friendly technology based on the oxidation of contaminants by strong oxidizing radicals, have received great attention. Among the AOPs, UV photolysis, UV/H_2O_2 photolysis, Fenton and photo-Fenton oxidation, heterogenous photocatalysis, and sonolysis have been applied for the removal of DP in aqueous solution. About 26% of the initial 5 μM of DP was eliminated under the UV irradiation (1272 mJ cm^{-2}), and adding 0.29 mM H_2O_2 in the photoreaction greatly improved the DP removal rate.[10] Photocatalytic degradation of DP by TiO_2 achieved 44.8% of DP removal under black blue lamps and 9.0% of mineralization under simulated solar radiation after 60 min irradiation, and the addition of H_2O_2 drastically improved the photocatalytic process, obtaining 100% DP degradation and 28.6% total organic carbon (TOC) reduction in UVC system.[11] Using iron oxide nanoparticles as catalyst *via* a photo-Fenton process, 100% of DP elimination and 83% of TOC reduction were obtained.[12] Heterogeneous photocatalysis using TiO_2 and its modified forms as catalysts also exhibited high efficiency in DP degradation and mineralization.[13,14] Ultrasonic irradiation at 640 kHz could effectively degrade DP in aqueous solution, and hydroxyl radical produced during cavitation played a crucial role in DP degradation.[15]

It appears that heterogeneous photocatalysis is a promising technique in water purification and wastewater treatment, with potential to achieve complete mineralization of organic pollutants into CO_2, water, and inorganic ions under solar irradiation.

[a]*School of Physics and Optoelectronic Engineering, Yangtze University, 1 Nanhuan Road, Jingzhou, Hubei 434023, China. E-mail: wqfscience@aliyun.com*

[b]*Department of Geosciences, University of Wisconsin-Parkside, 900 Wood Road, Kenosha, WI 53144, USA*

[c]*Faculty of Earth Sciences, China University of Geosciences, 388 Lumo Road, Wuhan, Hubei 430074, China*

† Electronic supplementary information (ESI) available. See DOI: 10.1039/d0ra07533g

Currently, design and utilization of novel photocatalytic materials have drawn great attention in the remediation of organic micropollutants and clean energy production.[16–20] Dolomite is an anhydrous carbonate mineral composed of calcium magnesium carbonate, with a ideal formula of $CaMg(CO_3)_2$. Natural dolomite often contains a certain amount of iron due to the partial substitution of Mg^{2+} by Fe^{2+} in the lattice.[21] As an industrial mineral, dolomite is widely used in food and pharmaceutical industries, production of fertilizers, glass and building materials, iron and steelmaking, and environmental remediation.[22] No studies on photocatalytic degradation of organic pollutants by natural dolomite and their modified forms have been reported in a recent literature search by the authors. As such, the main objectives of the present study were (1) to examine the possible catalytic effects of dolomite on the photodegradation of DP in aqueous solution, and evaluate its photocatalytic performance; (2) to identify the byproducts of DP in the photoreaction and speculate the possible photolytic pathways; and (3) to elucidate the intrinsic mechanisms for the photocatalytic activities of natural dolomite.

2. Experimental

2.1 Materials

The dolomite used in this study was supplied by XBKC Co., Ltd (Shiyan, China). The diphenhydramine hydrochloride with a purity > 98%, superoxide dismutase (SOD), and TiO_2 were provided by Sinopharm Chemical Reagent Co., Ltd (Shanghai, China). Acetonitrile, acetic acid, triethylamine, 1, 4-diazabicyclo [2.2.2] octane (DABCO), and isopropanol (IPA) were of high-performance liquid chromatography (HPLC) grade, and supplied by J&K Chemical Co., Ltd (Beijing, China). The spin-trapping reagents 5,5-dimethyl-1-pyrroline *N*-oxide (DMPO) and 2,2,6,6-tetramethylpiperidine (TEMP) were purchased from Sigma-Aldrich (Shanghai, China). All aqueous solutions were prepared with Milli-Q ultrapure water.

2.2 Pre-treatment and characterization of natural dolomite

The dolomite was first sieved to obtain a uniform 40–60 mesh sized particles. Then, the samples were washed with ultrapure water for three times, dried at 60 °C for 8 h, and stored in a desiccator for further use. No chemical treatments were made in order to maintain the natural attributes of dolomite. The morphology of samples were characterized using field emission scanning electron microscope (JEOL, JSM-6700) (Fig. S1†). The X-ray diffraction (XRD) pattern of the washed dolomite was recorded at 5° to 90° (2θ) using Bruker D8 advanced XRD instrument equipped with Cu-Kα radiation, and the collected XRD data were analyzed using MDI Jade 6.5 software. The elemental compositions of the dolomite were determined by a Rigaku-ZSX Primus II X-ray fluorescence (XRF) spectrometer. The results obtained from XRD (Fig. S2†) and XRF (Table 1) analysis indicate that it is an Fe-containing dolomite. The UV-vis diffuse reflectance spectra (DRS) of the dolomite were collected using a UV-vis spectrophotometer (UV2450, Shimadzu).

Table 1 Elemental compositions of natural dolomite determined by X-ray fluorescence spectrometer

Composition (%)								
CO_2	MgO	Al_2O_3	SiO_2	P_2O_5	SO_3	K_2O	CaO	Fe_2O_3
55.6	23.4	0.103	0.304	0.007	0.026	0.0171	20.5	0.0774

2.3 Photolysis experiments

Photoreaction was carried out in a PR22-25 photochemical reactor (PerfectLight, China) equipped with a 300 W xenon light source (PLS-SXE300UV) and a water-cooling system DC-0506 (HengPing, Shanghai). The spectral range of the xenon light source is 300–800 nm, and the light power entering the photoreactor was about 120 mW cm^{-2}. During the irradiation, the suspension was stirred continuously with the temperature kept at 4 °C by circulating water to prevent pyrolysis of DP. The reactor was airtight with a quartz glass plate on the open top of the vessel. In each experiment, 1.5 g dolomite sample was mixed with 200 mL DP solution (40 mg L^{-1}) in the 250 mL reactor, and then magnetically stirred for 30 min, then the suspension was irradiated under simulated solar light. At the given time intervals, a 2 mL aliquot of the suspension was collected, filtered through a 0.22 μm membrane, and analyzed by HPLC and LC-MS. Dark control experiments were conducted in the same manner as the regular experiments except that they were not exposed to light. All experiments were performed in duplicates to check the results.

2.4 Analytical determination and photoproduct identification

The concentration of DP in water was determined with a Shimadzu HPLC (LC-20) equipped with a C18 ODS reversed phase column (4.6 mm × 150 mm, 5 μm) and a SPD20 UV detector. The mobile phase consisted of 25 mM acetic acid and acetonitrile (60 : 40, v/v), with pH adjusted to 6.0 ± 0.1 using

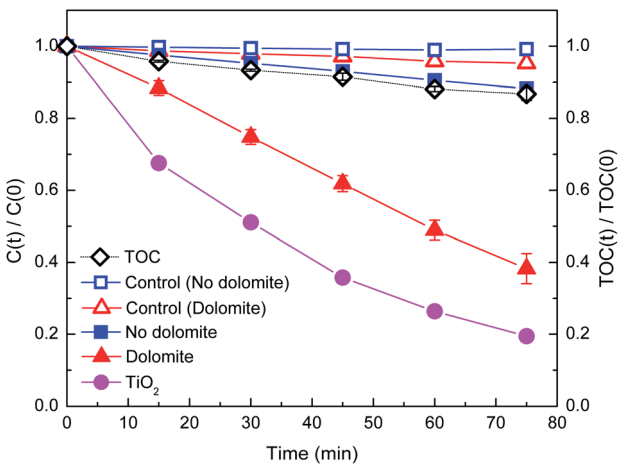

Fig. 1 Photodegradation and mineralization of DP in the presence of natural dolomite under simulated solar light, as well as the corresponding dark control. The added dolomite sample is 1.5 g per 200 mL of DP solution at an initial concentration of 40 mg L^{-1}.

Table 2 Fitted parameters for DP photodegradation under different reaction conditions by pseudo-first-order model

Reaction condition	K_{DP} (min^{-1})	R^2	$t_{1/2}$ (min)
No dolomite	$(0.16 \pm 0.01) \times 10^{-2}$	0.999	433.1
Dolomite	$(1.29 \pm 0.08) \times 10^{-2}$	0.982	53.7
TiO_2	$(2.16 \pm 0.05) \times 10^{-2}$	0.998	32.1
Dolomite + IPA	$(0.88 \pm 0.05) \times 10^{-2}$	0.99	78.7
Dolomite + SOD	$(0.82 \pm 0.04) \times 10^{-2}$	0.986	84.5
Dolomite + DABCO	$(1.03 \pm 0.04) \times 10^{-2}$	0.992	67.2
Dolomite + N_2	$(0.93 \pm 0.05) \times 10^{-2}$	0.99	74.5

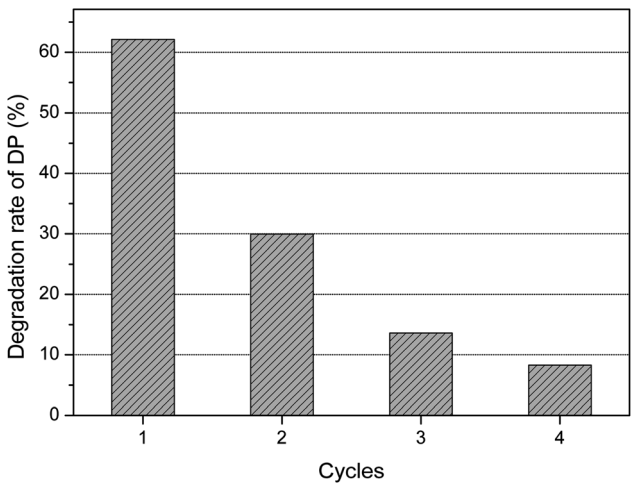

Fig. 2 Photocatalytic efficiency for the natural dolomite in the cycling experiments. The irradiation time is 75 min.

triethylamine. Isocratic elution was performed at a flow rate 0.8 mL min^{-1}. The injection volume was 20 μL. Oven temperature was kept at 30 °C and the detector wavelength was 220 nm.

Thermo Scientific Q Exactive mass spectrometer paired with the Ultimate 3000 LC system was used for the product studies. The analytical column was Agilent Zorbax XDB-C18 (2.1 mm × 50 mm, 1.8 μm). A mobile phase made of solvent A (0.1% formic acid in acetonitrile) and solvent B (0.1% formic acid in water) was used to elute the column with a flow rate 0.2 mL min^{-1} and the optimized gradient program 0–8 min, from 5% to 90% A; 8–10 min, 90% A. The column temperature was 30 °C. An injection volume of 5 μL was used for analytical samples. For MS detection, the operating parameters were as follows: spray voltage, 3200 V; capillary temperature, 300 °C; sheath gas pressure, 40 arb; aux gas pressure, 15 arb; S-lens RF, 50 V.

2.5 Determination of reactive species during photocatalytic degradation

In order to determine the reactive species in the photoreactions, electron spin resonance (ESR) signals for singlet oxygen, superoxide anions, and hydroxyl radicals trapped by TEMP and DMPO were obtained on a Bruker model ESP300E electron paramagnetic resonance spectrometer equipped with a Quanta-Ray Nd: YAG laser system as the irradiation light source ($\lambda = 355$ nm) at ambient temperature. The settings were center field at 3227.67 G; microwave frequency at 9054.62 MHz; and power at 0.998 mW. To further evaluate the role of these reactive species in the photodegradation of DP, reactive oxygen species (ROS) scavengers including DABCO ($^1O_2$ scavenger), IPA ($^{\bullet}OH$ scavenger) and SOD ($O_2^{-\bullet}$ scavenger) were used for the inhibition experiments.[23–25]

2.6 Theoretical calculations

To investigate the photocatalytic mechanism of DP under the catalysis of dolomite, the first-principle calculations were performed employing the VASP code (Vienna *Ab initio* Simulation Package).[26] The generalized gradient approximation (GGA) method with the Perdew–Burke–Ernzerhof (PBE) functional was used for the geometry optimization and electronic band structure calculations.[27,28] The kinetic energy cutoff was set as 500 eV, and a 4 × 4 × 1 *k*-point mesh was applied.[29] Optimization was performed with a convergence threshold for the maximum energy change of 1.0×10^{-5} eV per atom and for the maximum force of 0.01 eV $Å^{-1}$.

The experimental lattice constants of dolomite were $a = b =$ 4.81 Å, $c = 16.01$ Å, and the space group is $R\bar{3}$ (NO. 148).[30] The unit cell of dolomite in our calculations is composed of 6 C (gray), 18 O (red), 3 Mg (blue), and 3 Ca (green) atoms. And a supercell made of 2 × 2 × 1 was applied (Fig. S3(a)†). In order to simulate the partial substitution of Mg^{2+} by Fe^{2+} in natural dolomite, the Mg^{2+} ions in the unit cell are randomly replaced by Fe^{2+} ions (pink), with the Fe^{2+} number changing from 1 to 9. Fig. S3(b)† depicted the substitution of 3 Mg^{2+} by 3 Fe^{2+}.

3. Results and discussion

3.1 Photodegradation and mineralization of DP in the presence of natural dolomite

Fig. 1 illustrates the photodegradation of DP as a function of irradiation time in the presence and absence of natural dolomite, as well as the corresponding dark controls. For the dark control without dolomite, almost negligible loss of DP within 75 min indicated that the degradation by hydrolysis or thermal degradation could be neglected. While for the dark control with dolomite, approximately 4% of DP loss was detected, which could be attributed to physical adsorption to the surface of dolomite. When exposed to simulated solar light, DP in aqueous solution in the absence of dolomite was gradually decomposed with the irradiation time, and about 12% of DP removal was achieved after 75 min irradiation. A recent study reported DP removal of 32.5, 2.5, and 1.4% after 60 min irradiation under UVC, simulated solar light, and solar irradiation, respectively.[11] With the addition of dolomite into the solution, the DP removal increased to 62%, and the rate constant (K_{DP}) estimated from the pseudo-first order kinetic model increased from 0.16×10^{-2} to 1.29×10^{-2} min^{-1} (Table 2). Obviously, the presence of the natural dolomite greatly promoted the photodegradation of DP, exhibiting remarkable photocatalytic activity. The TOC reduction, an indication of mineralization, follows a similar trend as observed for DP degradation, about 14% of TOC elimination after 75 min irradiation indicated that

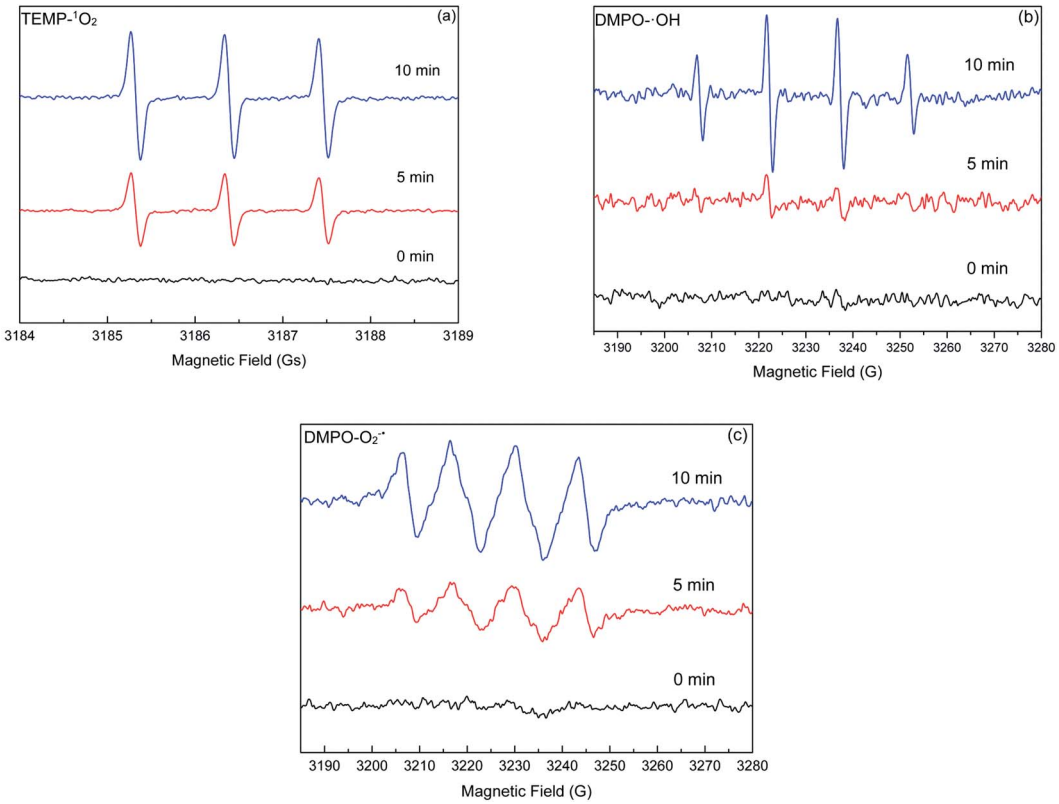

Fig. 3 ESR spectral changes of the TEMP–$^1O_2$ (a), DMPO–$^{\cdot}$OH (b), and DMPO–$O_2^{-\cdot}$ (c) adducts generated in the natural dolomite system under simulated solar light irradiation.

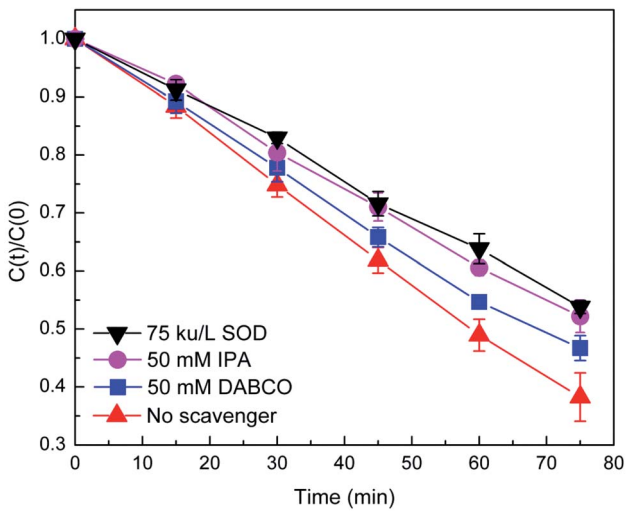

Fig. 4 Suppressed photodegradation of DP in the presence of natural dolomite by the radical scavengers. The initial concentration of IPA, DABCO, and SOD were 50, 50 mM, and 75 kU L^{-1}, respectively.

the dolomite photocatalytic process could effectively lead to the mineralization of DP (Fig. 1).

To further evaluate the photocatalytic performance of dolomite, photocatalytic degradation of DP by dolomite was compared to that by TiO_2 under the same conditions. Although the photocatalytic performance of dolomite was 19% lower than that by TiO_2, it could still be considered as a promising photocatalyst in the field of water treatment due to its much lower material cost, vast reserves, and environmental-friendly characters. Moreover, the recyclability and stability of the dolomite were evaluated through cycling experiments. As shown in Fig. 2, the degradation rate of DP was about 63% in the first cycle, and significantly decreased to 30% in the second cycle. After 4 cycles, the dolomite almost completely lost its photocatalytic activity. This result suggested that deactivation of the dolomite could occurred after several applications.

3.2 Study of reactive oxygen species

Photo-induced ROS, such as singlet oxygen ($^1O_2$), superoxide anion radical ($O_2^{-\cdot}$), and hydroxyl radical ($^{\cdot}$OH) were often considered as the main reactive species in photocatalytic processes. Therefore, it could be speculated that the enhanced DP degradation might also be due to the ROS produced in the dolomite system under irradiation. The EPR spin-trapping technique was deployed to examine the ROS generated in the photocatalytic process. The characteristic peaks of TEMP–$^1O_2$, DMPO–$O_2^{-\cdot}$, and DMPO–$^{\cdot}$OH adducts are observed in the dolomite system after irradiation, and the intensity of the peaks increased gradually with the irradiation time, while no signal was detected in the dark (Fig. 3). These evidences verified the generation of $^1O_2$, $O_2^{-\cdot}$, and $^{\cdot}$OH in the photocatalytic system.

In order to quantitatively evaluate the role of ROS in the present system, scavenger experiments were performed. In the

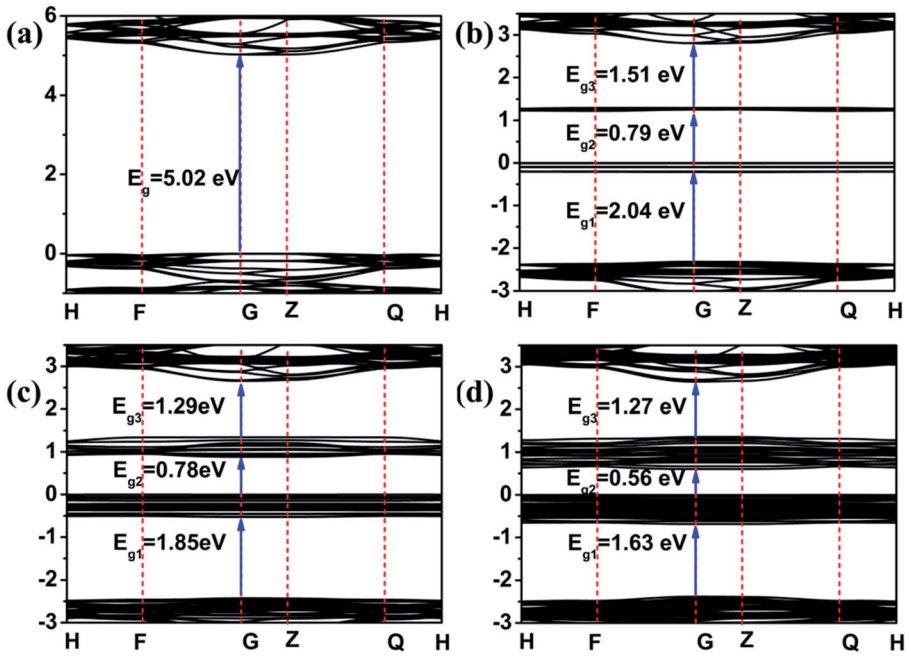

Fig. 5 Band structure for dolomite supercell with 0 (a), 3 (b), 6 (c), and 9 (d) Fe^{2+}-substitution. The Fermi level is set to 0.

presence of SOD ($O_2^{-\bullet}$ scavenger) and IPA ($^{\bullet}OH$ scavenger), DP photodegradation was significantly suppressed (Fig. 4), indicating the dominant role of the $O_2^{-\bullet}$ and $^{\bullet}OH$ in the photodegradation of DP. In contrast, the addition of DABCO ($^1O_2$ scavenger) showed a slight inhibition, which might be due to weak reactions between the amine drugs (including DP) and $^1O_2$.[31] Combining the EPR analyses and the radical scavenger experiments, it could be concluded that the $O_2^{-\bullet}$, $^1O_2$, and $^{\bullet}OH$ were the main reactive species responsible for the enhanced DP degradation in the presence of dolomite, and the $O_2^{-\bullet}$ and $^{\bullet}OH$ played the dominant role.

3.3 Mechanisms for photocatalytic activity of dolomite

In order to further elucidate the photocatalytic mechanism, density functional theory (DFT) was employed to calculate the electronic band structure and density of states (DOS) for dolomite. The calculated band gap of the pristine dolomite is 5.02 eV, consistent with a previous report of 5.035 eV (Fig. 5(a)).[32] With 3 Fe^{2+} substitution, two new bands appear in the band structures, resulting in forbidden band gap being divided into three parts (Fig. 5(b)). Among them, the maximum band gap is 2.04 eV. With the increase of Fe^{2+}content, more energy levels appear in the forbidden band gap, and the new bands become wider, leading to reduction of the band gap. After 9 Fe^{2+} substitution, the maximum band gap decreased to 1.63 eV (Fig. 5(d)), close to the band gap calculated from the UV-vis reflectance spectra (1.33 eV) of dolomite (Fig. S4†). The change in band gap of dolomite from 5.02 to 1.63 eV implies that the dolomite changes from an insulator to a semiconductor with partial substitution of Mg^{2+} by Fe^{2+}.

The DOS calculation indicated that the states near the valence band maximum (VBM) are contributed by the hybrid

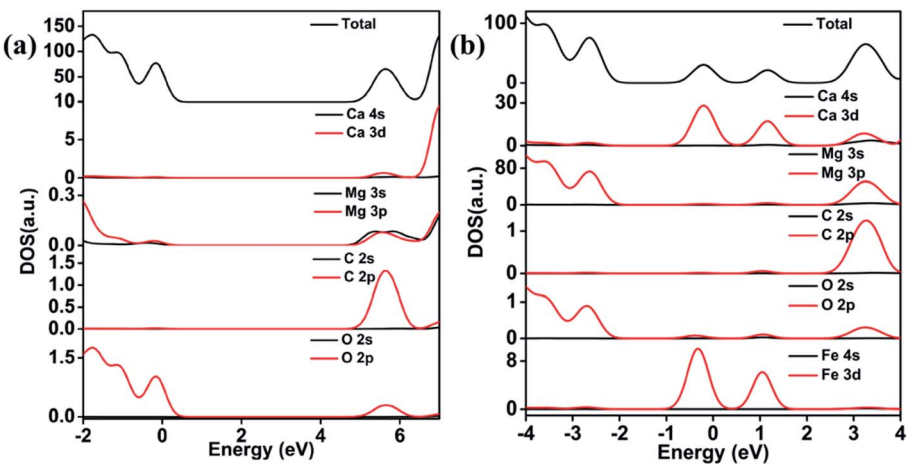

Fig. 6 Density of state for pure (a) and 3 Fe^{2+}-substituted (b) dolomite. The Fermi level is set to 0.

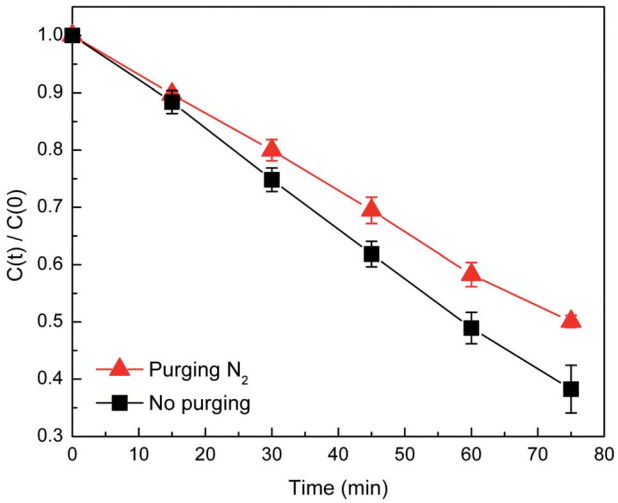

Fig. 7 The photodegradation of DP in the presence of natural dolomite in the deoxygenated solution.

between O 2p and Mg 3p orbitals, and the states near the conduction band maximum (CBM) mainly originate from C 2p and Ca 3d orbitals for the pristine dolomite (Fig. 6(a)). Two additional doping states appear in the forbidden band gap after 3 Fe^{2+} substitution, which is attributed to the hybrid between Fe 3d and Ca 3d orbitals (Fig. 6(b)). With the increase of Fe^{2+} contents, the two doping states become wider, thereby resulting in gradual decrease of the band gap.

Overall, the theoretical calculation results indicate that the dolomite exhibits the characters of semiconductors after the substitution of Mg^{2+} by Fe^{2+}, suggesting that dolomite could act as a semiconductor photocatalyst under the irradiation of solar light. To verify the role of O_2 during the photocatalytic process, deoxygenation experiments were performed and the DP degradation was suppressed by N_2 purging (Fig. 7). The generation of ROS in the dolomite system was related to the dissolved oxygen (DO) in solution. N_2 purging causes a decrease of DO concentration, thus inhibiting the formation of reactive oxygen species.

Table 3 Retention time, mass spectra, and structure of the identified photoproducts

m/z	Retention time (min)	Elemental composition	Proposed structure
167	7.1	$C_{13}H_{11}$	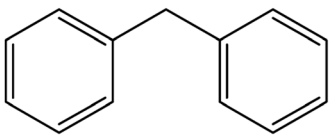
183	8.0	$C_{13}H_{11}O_2$	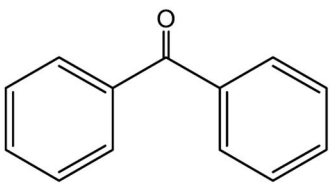
256	5.8	$C_{17}H_{22}NO$	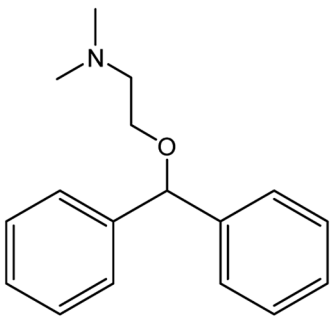
272	6.0	$C_{17}H_{22}NO_2$	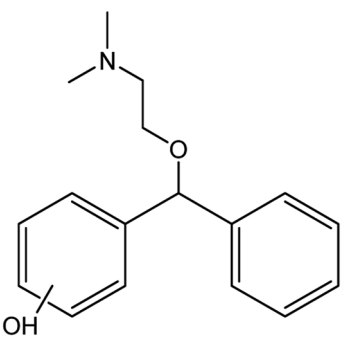

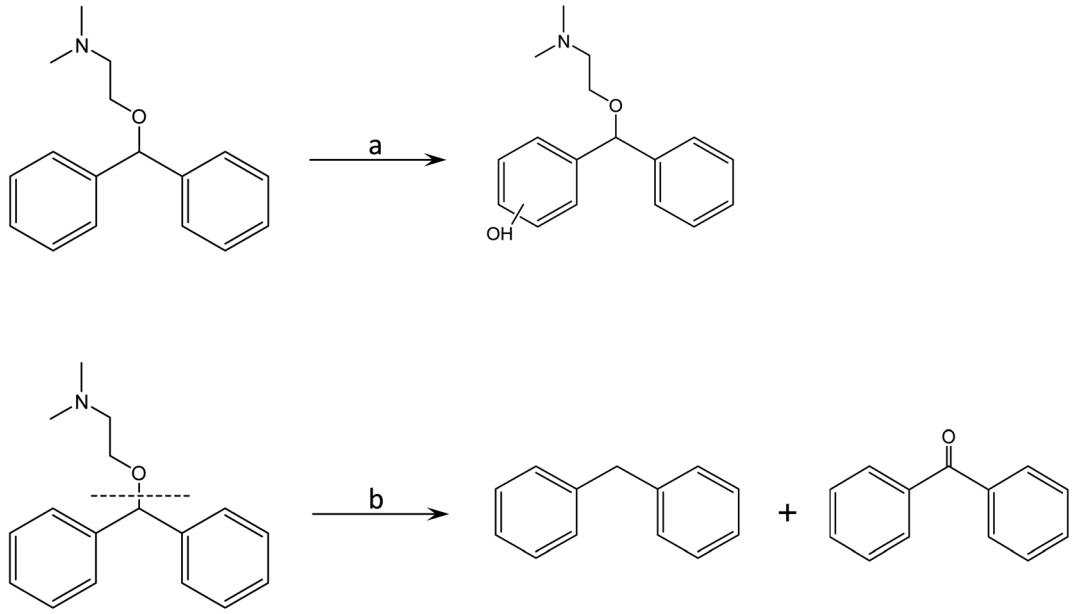

Fig. 8 Proposed degradation pathways of DP in the presence of natural dolomite.

According to the theoretical calculations, the results from ESR analysis, and the deoxygenation experiments, we proposed a mechanism for the photocatalysis of dolomite. Under irradiation, photo-excited electrons and holes migrate to the surface of the dolomite (eqn (1)). Subsequently, further reactions according to eqn (2)–(6) yield $^{\cdot}OH$ and $O_2^{-\cdot}$. As for $^1O_2$, its generation might be due to the energy transfer between dolomite and DO.

$$\text{Dolomite} + h\nu \rightarrow h^+ + e^- \quad (1)$$

$$H_2O + h^+ \rightarrow {}^{\cdot}OH + H^+ \quad (2)$$

$$O_2 + e^- \rightarrow O_2^{-\cdot} \quad (3)$$

$$O_2^{-\cdot} + H^+ \rightarrow HO_2^{\cdot} \quad (4)$$

$$2HO_2^{\cdot} \rightarrow H_2O_2 + O_2 \quad (5)$$

$$H_2O_2 + O_2^{-\cdot} \rightarrow {}^{\cdot}OH + OH^- + O_2 \quad (6)$$

3.4 Identification of degradation products and pathways

To obtain a further insight into the photolytic mechanism and the photochemical fate of the DP, the main degradation products of DP in the reaction were identified using HR LC-MS, respectively (Fig. S5†). As shown in Table 3, the photocatalytic process leads to the formation of *m*/*z* 183, *m*/*z* 272, and *m*/*z* 167, which were also detected in the previous studies.[15,31,33]

Among the observed products, *m*/*z* of 272 could be attributed to the hydroxylation of DP (*m*/*z* 256) (Fig. 8). Hydroxyl radical is a strong electrophilic species, and readily adds to aromatic rings. Thus, hydroxyl radical addition to the aromatic ring accompanied by dehydrogenation is a common reaction pathway for aromatic compounds.[15] Considering the generation of $^{\cdot}OH$ in the dolomite system, it is logical to expect the addition of $^{\cdot}OH$ to the aromatic ring in DP molecules, leading to the formation of *m*/*z* 272. As for the products of *m*/*z* 183 and 167, their formation might result from the hydroxyl radical mediated oxidation of the alkylamine side chain (Fig. 8).[32,33]

In summary, from the intermediates determined it appears that the oxidation process occurs mainly through the hydroxyl radicals. However, the results from the scavenger experiments indicated that the superoxide anions also play an important role. Thus, it seems that the superoxide anions generated were converted to hydroxyl radicals *via* further reaction, reinforcing the role of hydroxyl radicals.

4. Conclusions

For the first time, dolomite, an inexpensive and easily available mineral, was used for photocatalytic degradation of DP in aqueous solution. The results demonstrated that the presence of dolomite greatly promoted the degradation of DP, exhibiting significant photocatalytic activity. The ESR analysis and scavenger experiments demonstrated that $^1O_2$, $O_2^{-\cdot}$, and $^{\cdot}OH$ were produced in the dolomite system after irradiation, and contributed to the enhanced DP photodegradation. Based on the first-principles calculations, it was proposed that the process of dolomite photocatalysis mainly involved in two steps: first, the dolomite with semiconductor properties produces photo-generated electrons and holes under irradiation, which subsequently react to form reactive species. Second, the reactive species such as hydroxyl radicals caused the oxidation of DP. The product studies indicated, on the one hand, that the hydroxylation of aromatic rings and oxidation of the alkylamine side chain are the main degradation pathways of DP; while, on the other hand, the hydroxyl radicals are produced in the photocatalytic process and play an important role in DP degradation.

Conflicts of interest

There are no conflicts to declare.

Acknowledgements

This work was supported by the National Natural Science Foundation of China (Grant 41403083), the Key Project of Science and Technology of Hubei Provincial Department of Education (Grant D20141305) and Natural Science of Foundation of Hubei Province, China (Grant 2019CFB225).

References

1 Q. Bu, B. Wang, J. Huang, S. Deng and H. Yu, Pharmaceuticals and personal care products in the aquatic environment in China: a review, *J. Hazard. Mater.*, 2013, **262**, 189–211.

2 L. Arpin-Pont, M. J. M. Bueno, E. Gomez and H. Fenet, Occurrence of PPCPs in the marine environment: a review, *Environ. Sci. Pollut. Res.*, 2016, **23**, 4978–4991.

3 Y. Yang, Y. S. Ok, K. H. Kim, E. E. Kwon and Y. F. Tsang, Occurrences and removal of pharmaceuticals and personal care products (PPCPs) in drinking water and water/sewage treatment plants: a review, *Sci. Total Environ.*, 2017, **596–597**, 303–320.

4 P. K. Jjemba, Excretion and ecotoxicity of pharmaceutical and personal care products in the environment, *Ecotoxicol. Environ. Saf.*, 2006, **63**, 113–130.

5 S. A. Ortiz de Garciá, G. P. Pinto, P. A. García-Encina and R. Irusta-Mata, Ecotoxicity and environmental risk assessment of pharmaceuticals and personal care products in aquatic environments and wastewater treatment plants, *Ecotoxicology*, 2014, **23**, 1517–1533.

6 L. Cizmas, V. K. Sharma, C. M. Gray and T. J. McDonald, Pharmaceuticals and personal care products in waters: occurrence, toxicity, and risk, *Environ. Chem. Lett.*, 2015, **13**, 381–394.

7 J. P. Berninger, B. Du, K. A. Connors, S. A. Eytcheson, M. A. Kolkmeier, K. N. Prosser, T. W. Valenti Jr, C. K. Chambliss and B. W. Brooks, Effects of the antihistamine diphenhydramine on selected aquatic organisms, *Environ. Toxicol. Chem.*, 2011, **30**, 2065–2072.

8 B. Du, A. E. Price, W. C. Scott, L. A. Kristofco, A. J. Ranirez, C. K. Chambliss, J. C. Yederman and B. W. Brooks, Comparison of contaminants of emerging concern removal, discharge, and water quality hazards among centralized and on-site wastewater treatment system effluents receiving common wastewater influent, *Sci. Total Environ.*, 2014, **466–467**, 976–984.

9 P. E. Stackelberg, E. T. Furlong, M. T. Meyer, S. D. Zaugg, A. K. Henderson and D. B. Reissman, Persistence of pharmaceutical compounds and other organic wastewater contaminants in a conventional drinking-water-treatment plant, *Sci. Total Environ.*, 2004, **329**, 99–113.

10 F. Yuan, C. Hu, X. Hu, J. Qu and M. Yang, Degradation of selected pharmaceuticals in aqueous solution with UV and UV/H_2O_2, *Water Res.*, 2009, **43**, 1766–1774.

11 N. López, P. Marco, J. Giménez and S. Esplugas, Photocatalytic diphenhydramine degradation under different radiation sources: kinetic studies and energetic comparison, *Appl. Catal., B*, 2018, **220**, 497–505.

12 L. M. Pastrana-Martínez, N. Pereira, R. Lima, J. L. Faria, H. T. Gomes and A. M. T. Silva, Degradation of diphenhydramine by photo-Fenton using magnetically recoverable iron oxide nanoparticles as catalyst, *Chem. Eng. J.*, 2015, **261**, 45–52.

13 L. M. Pastrana-Martínez, J. L. Faria, J. M. Doña-Rodríguez, C. Fernández-Rodríguez and A. M. T. Silva, Degradation of diphenhydramine pharmaceutical in aqueous solutions by using two highly active TiO_2 photocatalysts: operating parameters and photocatalytic mechanism, *Appl. Catal., B*, 2012, **113–114**, 221–227.

14 S. Morales-Torres, L. M. Pastrana-Martínez, J. L. Figueiredo, J. L. Faria and A. M. T. Silva, Graphene oxide-P25 photocatalysts for degradation of diphenhydramine pharmaceutical and methyl orange dye, *Appl. Surf. Sci.*, 2013, **275**, 361–368.

15 D. Cui, A. M. Mebel, L. E. Arroyo-Mora, C. Zhao, A. D. Caprio and K. O'Shea, Fundamental study of the ultrasonic induced degradation of the popular antihistamine, diphenhydramine (DPH), *Water Res.*, 2018, **144**, 265–273.

16 A. Xu, W. Tu, S. Shen, Z. Lin, N. Gao and W. Zhong, $BiVO_4$@MoS_2 core–shell heterojunction with improved photocatalytic activity for discoloration of Rhodamine B, *Appl. Surf. Sci.*, 2020, **528**, 146949.

17 Z. Wang, B. Xiao, Z. Lin, S. Shen, A. Xu, Z. Du, Y. Chen and W. Zhong, *In situ* surface decoration of RuO_2 nanoparticles by laser ablation for improved oxygen evolution reaction activity in both acid and alkali solutions, *J. Energy Chem.*, 2021, **54**, 510–518.

18 W. Zhong, S. Shen, M. He, D. Wang, Z. Wang, Z. Lin, W. Tu and J. Yu, The pulsed laser-induced Schottky junction *via in situ* forming Cd clusters on CdS surfaces toward efficient visible light-driven photocatalytic hydrogen evolution, *Appl. Catal., B*, 2019, **258**, 117967.

19 P. Shao, J. Tian, X. Duan, Y. Yang, W. Shi, X. Luo, F. Cui, S. Luo and S. Wang, Cobalt silicate hydroxide nanosheets in hierarchical hollow architecture with maximized cobalt active site for catalytic oxidation, *Chem. Eng. J.*, 2019, **359**, 79–87.

20 P. Shao, J. Pei, H. Tang, S. Yu, L. Yang, H. Shi, K. Yu, K. Zhang and X. Luo, Defect-rich porous carbon with anti-interference capability for adsorption of bisphenol A *via* long-range hydrophobic interaction synergized with short-range dispersion force, *J. Hazard. Mater.*, 2021, **403**, 123705.

21 R. J. Reeder and W. A. Dollase, Structural variation in the dolomite-ankerite solid-solution series: an X-ray, Mössbauer, and TEM study, *Am. Mineral.*, 1989, **74**, 1159–1167.

22 O. Sivrikaya, A study on the physicochemical and thermal characterisation of dolomite and limestone samples for use in ironmaking and steelmaking, *Ironmaking Steelmaking*, 2018, **45**, 764–772.

23 P. Shao, S. Yu, X. Duan, L. Yang, H. Shi, L. Ding, J. Tian, L. Yang, X. Luo and S. Wang, Potential difference driving electron transfer *via* defective carbon nanotubes toward selective oxidation of organic micropollutants, *Environ. Sci. Technol.*, 2020, **54**, 8464–8472.

24 P. Shao, X. Duan, J. Xu, J. Tian, W. Shi, S. Gao, M. Xu, F. Cui and S. Wang, Heterogenous activation of peroxymonosulfate by amorphous boron for degradation of bisphenol S, *J. Hazard. Mater.*, 2017, **322**, 532–539.

25 P. Shao, J. Tian, F. Yang, X. Duan, S. Gao, W. Shi, X. Luo, F. Cui, S. Luo and S. Wang, Identification and regulation of active sites on nanodiamonds: establishing a highly efficient catalytic system for oxidation of organic contaminants, *Adv. Funct. Mater.*, 2018, **28**, 1705295.

26 G. Kresse and J. Furthmüller, Efficiency of *ab initio* total energy calculations for metals and semiconductors using a plane-wave basis set, *Comput. Mater. Sci.*, 1996, **6**, 15–50.

27 B. Hammer, L. B. Hansen and J. K. Norskov, Improved adsorption energetics within density-functional theory using revised Perdew-Burke-Ernzerhof functionals, *Phys. Rev. B: Condens. Matter Mater. Phys.*, 1999, **59**, 7413–7421.

28 W. Zhang and Y. Xiao, Mechanism of electrocatalytically active precious Metal (Ni, Pd, Pt, and Ru) complexes in the graphene basal plane for ORR applications in novel fuel cells, *Energy Fuels*, 2020, **34**, 2425–2434.

29 Q. Wang, Z. Q. Liu, D. M. Liu, W. Wang, Z. W. Zhao, F. Y. Cui and G. B. Li, Oxygen vacancy-rich ultrathin sulfur-doped bismuth oxybromide nanosheet as a highly efficient visible-light responsive photocatalyst for environmental remediation, *Chem. Eng. J.*, 2019, **360**, 838–847.

30 J. Warren, Dolomite: occurrence, evolution and economically important associations, *Earth-Sci. Rev.*, 2000, **52**, 1–81.

31 Y. Chen, C. Hu, X. Hu and J. Qu, Indirect photodegradation of amine drugs in aqueous solution under simulated sunlight, *Environ. Sci. Technol.*, 2009, **43**, 2760–2765.

32 F. M. Hossain, G. E. Murch, I. V. Belova and B. D. Turner, Electronic, optical and bonding properties of $CaCO_3$ calcite, *Solid State Commun.*, 2009, **149**, 1201–1203.

33 N. López, S. Plaza, A. Afkhami, P. Marco, J. Giménez and S. Esplugas, Treatment of diphenhydramine with different AOPs including photo-Fenton at circumneutral pH, *Chem. Eng. J.*, 2017, **318**, 112–120.